Tectonophysics 690 (2016) 160–173

Contents lists available at ScienceDirect

Tectonophysics

journal homepage: www.elsevier.com/locate/tecto

Effective crustal permeability controls fault evolution: An integrated structural, mineralogical and isotopic study in granitic gneiss, Monte Rosa, northern Italy

Susan E.M. Lawther [a,*], Tim J. Dempster [a], Zoe K. Shipton [b], Adrian J. Boyce [c]

[a] School of Geographical and Earth Sciences, University of Glasgow, Glasgow G12 8QQ, UK
[b] Department of Civil and Environmental Engineering, University of Strathclyde, Glasgow G1 1XJ, UK
[c] NERC Isotope Community Support Facility, Scottish Universities Environmental Research Centre, East Kilbride G75 0QF, UK

ARTICLE INFO

Article history:
Received 8 October 2015
Received in revised form 1 July 2016
Accepted 15 July 2016
Available online 18 July 2016

Keywords:
Fault evolution
Fluid flow
Stable isotopes
Permeability
Fluid–rock reactions
Granitic basement

ABSTRACT

Two dextral faults within granitic gneiss in the Monte Rosa nappe, northern Italy reveal key differences in their evolution controlled by evolving permeability and water/rock reactions. The comparison reveals that identical host rock lithologies develop radically different mineralogies within the fault zones, resulting in fundamentally different deformation histories. Oxygen and hydrogen isotope analyses coupled to microstructural characterisation show that infiltration of meteoric water occurred into both fault zones. The smaller Virgin Fault shows evidence of periodic closed system behaviour, which promoted the growth of hydrothermal K-feldspar, whilst the more open system behaviour of the adjacent Ciao Ciao Fault generated a weaker muscovite-rich fault core, which promoted a step change in fault evolution. Effective crustal permeability is a vital control on fault evolution and, coupled to the temperature (i.e. depth) at which key mineral transformations occur, is probably a more significant factor than host rock strength in controlling fault development. The study suggests that whether a fault in granitic basement grows into a large structure may be largely controlled by the initial hydrological properties of the host rocks. Small faults exposed at the surface may therefore be evolutionary "dead-ends" that typically do not represent the early stages in the development of larger faults.

Fault zones are long-lived zones of weakness in the Earth's crust; how they form and evolve is crucial to studies of earthquake mechanics and subsurface fluid flow (Martel, 1990; Cavailhes et al., 2013). In faults within basement rocks, the damage zone generally has high permeability compared to both the host rock and the fault core (Caine et al., 1996; Evans et al., 1997), however the permeability of the fault core and damage zone will vary as successive deformation events create new fractures or re-open existing fractures (Caine et al., 1996; Zhang and Tullis, 1998). Fracturing and cataclasis cause grain size reduction and generate weaker rocks that can be deformed more easily by granular flow/cataclasis (Tullis and Yund, 1985). Hence as deformation proceeds, mechanisms may switch from discrete fracturing to cataclasis (Fitzgerald and Stünitz, 1993). Fracturing creates higher permeability and the presence of fluids in a fault zone may control the mineralogy via fluid–rock reactions (Chester et al., 1993; Wintsch et al., 1995), which in turn influences the deformation mechanisms and fault rock strength (Janecke and Evans, 1988; Wibberley, 1999; Di Toro and Pennacchioni, 2005; Faulkner et al., 2008; Boulton et al., 2009). Depending on the nature of the reactions; porosity can be created or destroyed, permeability increased or decreased and these characteristics, in turn, can affect seismic processes (Wintsch et al., 1995; Janssen et al., 1998; Kirkpatrick and Shipton, 2009; Mittempergher et al., 2009).

This paper describes the relationships between mineralogy, fluid influx and deformation history on two adjacent but contrasting Alpine faults in granitic gneiss from the Monte Rosa nappe, northern Italy using a combination of field and petrographic evidence, fluid inclusion and stable isotope analysis. We develop a model for fault development that links the evolving hydraulic properties of the fault to the mineral reactions controlling rock strength.

1. Geological setting

The field area, Passo Moro, is within the Monte Rosa nappe of the Western Alps, northern Italy. The area consists of granitic gneiss, amphibolite and an approximately 150 m thick metasedimentary layer primarily composed of quartz-rich pelites (Fig. 1A). Both the granitic gneiss and pelites have a foliation defined by muscovite and biotite dipping at ca. 35° to the WNW. The largest amphibolite sheet can be traced for 300–400 m. Several other thin amphibolites are below the resolution of the map. The Macugnaga augen gneiss was originally emplaced as a

* Corresponding author at: Banah UK Ltd, 1B Letterloan Rd, Macosquin, Coleraine BT51 4PP, UK.
E-mail address: susan.l@banahuk.co.uk (S.E.M. Lawther).

http://dx.doi.org/10.1016/j.tecto.2016.07.010

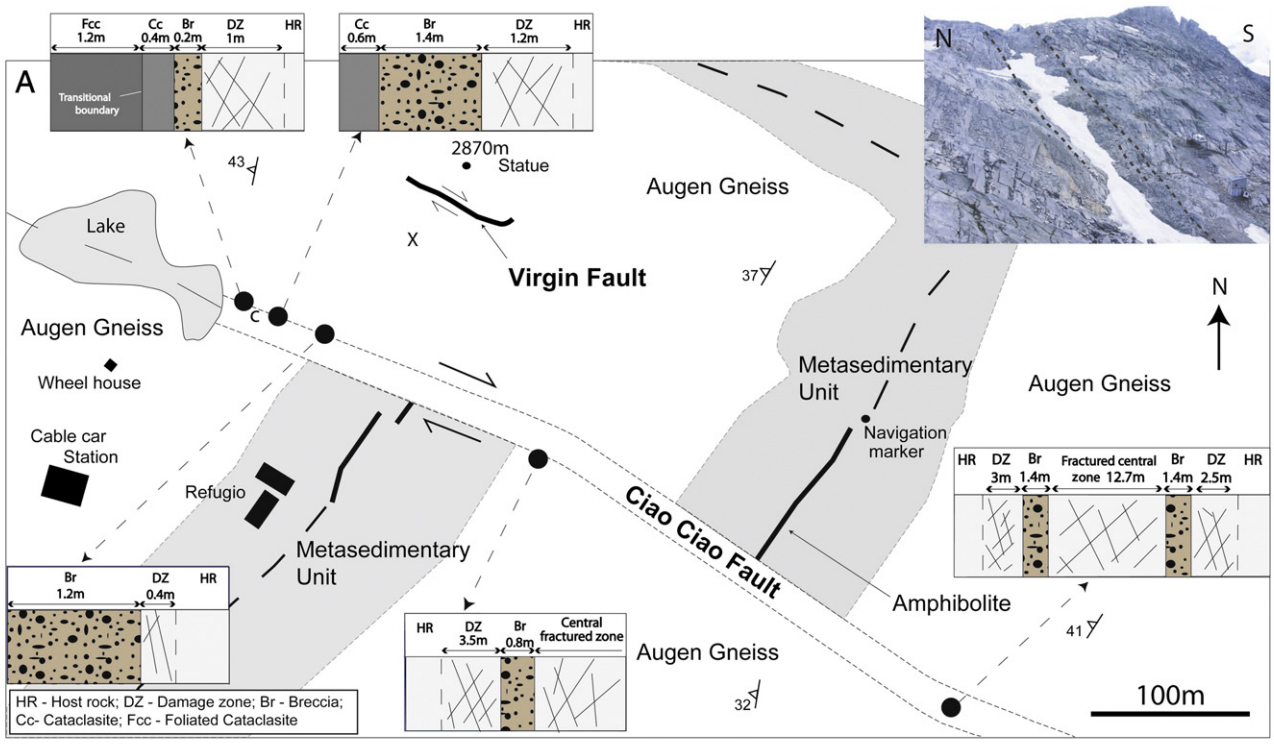
A
Fcc 1.2m
Cc 0.4m
Br 0.2m
DZ 1m
HR
Transitional boundary
Cc 0.6m
Br 1.4m
DZ 1.2m
HR
N
S
2870m
Statue
Augen Gneiss
Lake
X
Virgin Fault
37
N
Augen Gneiss
C
Wheel house
Metasedimentary Unit
Augen Gneiss
Cable car Station
Navigation marker
HR DZ 3m Br 1.4m Fractured central zone 12.7m Br 1.4m DZ 2.5m HR
Refugio
Ciao Ciao Fault
Br 1.2m
DZ 0.4m
HR
Metasedimentary Unit
Amphibolite
41
HR DZ 3.5m Br 0.8m Central fractured zone
Augen Gneiss
32
100m
HR - Host rock; DZ - Damage zone; Br - Breccia;
Cc- Cataclasite; Fcc - Foliated Cataclasite

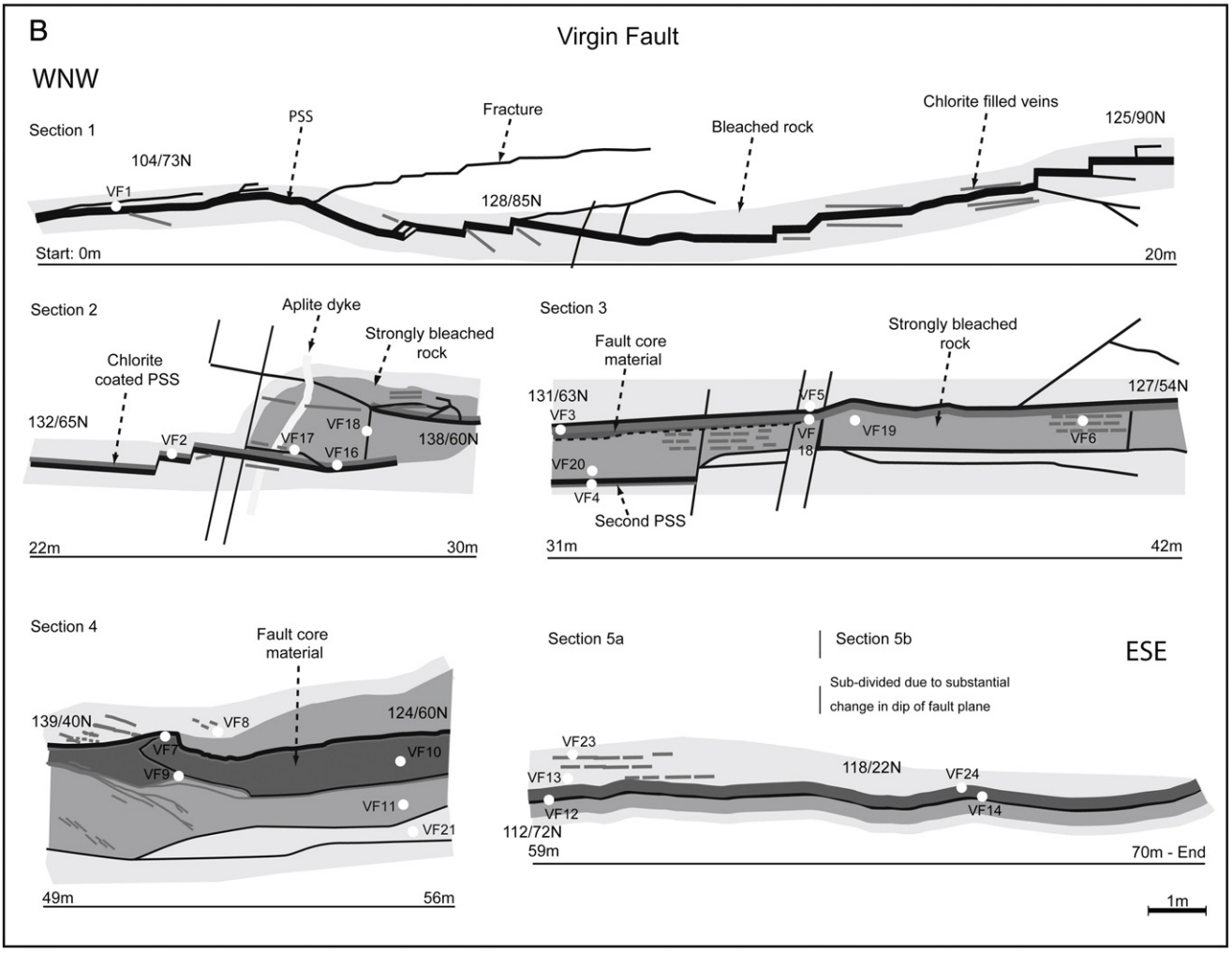
B
Virgin Fault
WNW
Section 1
104/73N
PSS
Fracture
Bleached rock
Chlorite filled veins
125/90N
VF1
128/85N
Start: 0m
20m
Section 2
Aplite dyke
Strongly bleached rock
Chlorite coated PSS
132/65N
VF2
VF17
VF18
VF16
138/60N
22m
30m
Section 3
Fault core material
Strongly bleached rock
131/63N
VF3
VF5
VF
18
VF19
VF6
127/54N
VF20
VF4
Second PSS
31m
42m
Section 4
Fault core material
139/40N
VF8
124/60N
VF7
VF9
VF10
VF11
VF21
49m
56m
Section 5a
Section 5b
ESE
Sub-divided due to substantial change in dip of fault plane
VF23
VF13
118/22N
VF24
VF12
VF14
112/72N
59m
70m - End
1m

granite pluton at 260 Ma (Bearth, 1952; Frey et al., 1976). The main Alpine metamorphic event climaxed at 38 Ma (Bocquet et al., 1974; Amato et al., 1999) and grades from greenschist facies in the SW to amphibolite facies in the NE (Dal-Piaz et al., 1972). At ca. 33 Ma the Monte Rosa nappe was at a depth of ~11–15 km (Berger and Bousquet, 2008) and subsequent deformation was dominated by brittle faulting (Hurford et al., 1991). The Monte Rosa nappe has experienced no subsequent regional metamorphic events; and mineral changes within the fault zones are therefore a result of fluid–rock reactions during exhumation.

The earliest phase of faulting at Monte Rosa was synchronous with formation of gold lodes at 33 Ma (Curti, 1987; Lattanzi et al., 1989). The Pestarena gold veins near Macugnaga have been dated at 29 Ma and are believed to have formed at 240–350 °C and ~5–12 km depth (Pettke et al., 1999). Frey et al. (1976) determined stable isotopic compositions of the gneisses and recorded evidence for Alpine resetting. $\delta^{18}O_{Fluid}$ results show a high degree of uniformity and the majority of δD_{Fluid} values fall into the range of −40 to −80‰, considered as 'normal' for igneous rocks. With regards to the metamorphic fluids they found no evidence for significant input of oxygen from external sources and thus Monte Rosa 'stewed in its own juices'. Frey et al. (1976) argued that two δD_{Fluid} values outside this range (−134 and −157‰) implied some limited interaction with a meteoric fluid.

Many small faults are exposed in the area, but this study focuses on two dextral strike-slip fault zones: the Virgin Fault and the Ciao Ciao Fault. The former has accumulated ~10 cm of displacement while the latter has accumulated ~250 m of displacement (calculated by the offset of an aplite dyke and amphibolite sheet respectively, Fig. 1). Four dominant joint sets are oriented approximately 040/85 N; 090/90; 146/74NE and 010/33 W (Fig. 2). The latter are parallel to foliation. The 146/74NE joints are approximately fault parallel and have locally been reactivated as faults. Such planes may have slickenlines with a mean plunge of 11° towards 117° and are coated with quartz and/or chlorite and/or epidote. Joint density, determined by linear scan lines, varies within the augen gneiss on a m-scale from 0.2/m to 7/m with a mean of 2/m. Higher joint densities occur adjacent to the faults.

2. The Virgin Fault

The Virgin Fault is a 70 m long right-lateral strike-slip fault (Fig. 1B). The principal slip surface has a mean orientation of 132/70 N (Fig. 2). The Virgin Fault is an isolated fault that has no evidence of interaction with other faults in the plane of the outcrop. Slickenlines record strike-slip motion (e.g. 2° towards 103° and 24° towards 133°) (Fig. 2). In the host granitic gneisses around the fault, the average density of the joints that strike at 090°, 146° and 040° is 1.2/m. None of the 090 joints intersect the fault. The foliation parallel joints do intersect the fault; their density increases from background levels of 0.5/m to ~4/m at 45 to 55 m along strike of the Virgin Fault. The dominant fracture orientation in the damage zone is fault parallel, but orientations vary from ca. 117–151° and dip from 22 to 87°. 040/90 fractures also occur in the fault zone but cross-cutting relationships indicate that they formed after faulting.

The Virgin Fault is composed of a central principal slip surface and/or fault core surrounded by a damage zone. The fault core is characterised by brecciation, cataclasis, retrograde reaction products and mineral precipitation (Fig. 3). The damage zone is characterised by bleaching and an increased fracture density compared to the host rock. Fault width, defined by the width of the core plus the damage zone, increases from 5 cm at the tips, to 3.2 m at ~55 m from the western tip. The polished principal slip surface is semi-continuous with mineralised

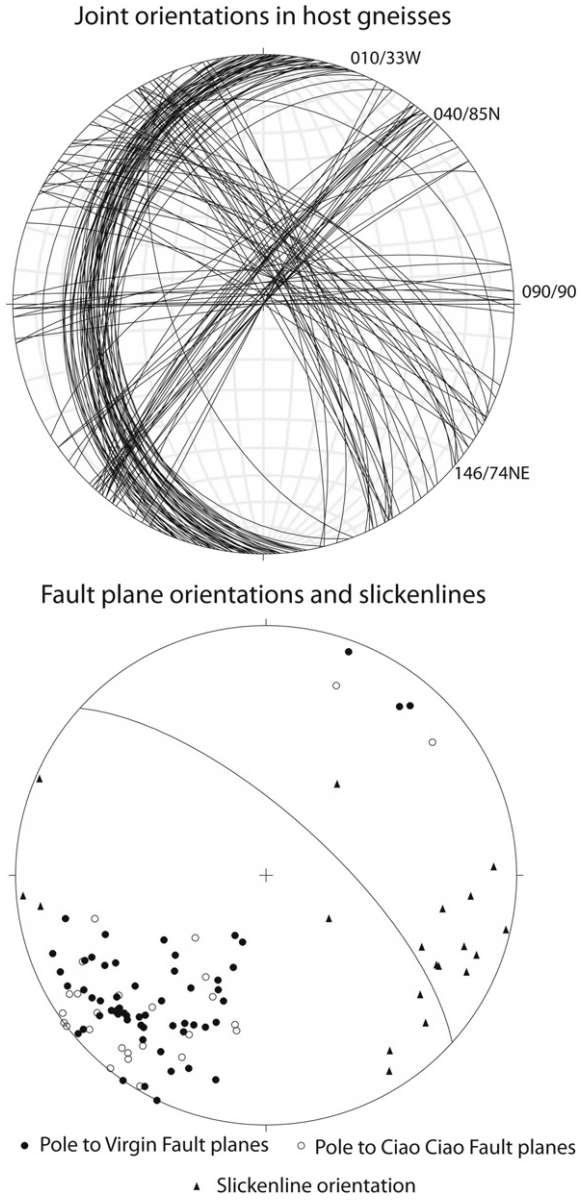

Fig. 2. Equal area stereonets showing orientations of 4 sets of joint planes within the host gneiss and measured orientations (poles to planes) of the fault surfaces for the Virgin and Ciao Ciao Faults. Average orientation of Virgin Fault shown as great circle. Orientations of slickenlines for both faults are also plotted.

areas containing quartz and/or chlorite and/or epidote. Slip surfaces are typically steeply inclined, slightly curved and consistently link in a left-stepping sense (Fig. 1B). Towards the eastern end of the fault, the dip shallows to 22°. The fault core is present from ~20 m along strike to the eastern tip (Fig. 1B). The core varies in thickness from 3 mm to 75 cm and is typically composed of white feldspar and quartz fragments in a dark green, fine grained chlorite and/or epidote matrix.

Bleaching occurs within ca. 50 cm of the principal slip surface: its intensity progressively increases from 0 m to 35 m along strike, and from 35 m to the eastern tip the intensity of bleaching is consistently strong. Chlorite veins occur throughout the strongly bleached damage zone (Fig. 3A and B); veins of epidote tend to be restricted to sections 2 and 3 (Fig. 1B). Chlorite veins are 5 mm to 30 cm long and aperture varies

Fig. 1. A) Geological map of the Passo Moro area showing trace of the Virgin and Ciao Ciao Faults. Insets show schematic cross sections of structures at locations along the Ciao Ciao Fault and field photograph taken from point x looking SE along the trace of the fault, the snow-filled gulley marked by the dashed lines is approximately 15 m wide. Location c marks position of fault rocks shown in Fig. 3c. Cable car station is located at Lat 49°59′48.2″; Long 07°58′37.8″. B) Map of the Virgin Fault along NNW-SSE transect showing areas of chlorite veining and bleaching, together with sample locations. Gaps between sections are caused by areas of no exposure. Orientations of slip surfaces are shown.

Fig. 3. Field photographs of fault rocks. A) Core of the Virgin Fault showing breccia (Br) and cataclasite (Ca) adjacent to bleached damage zone rock (DZ) sample VF14 (Fig. 1B); B) Chlorite-coated principal slip surface in the Virgin Fault adjacent to bleached and veined damage zone (DZ), sample VF2; C) Surface expression of the Ciao Ciao Fault at location c (Fig. 1A), showing transition from host rock (HR) -damage zone (DZ) -breccia (Br) -cataclasite (Cc) -foliated cataclasite (Fcc). Compass-clino (centre) for scale. Two principal slip surfaces occur within the Ciao Ciao Fault at this locality. Dashed lines represent transitional boundaries.

from approximately 1 mm to 2.5 cm; they are shorter, thinner and more isolated near the western tip.

3. The Ciao Ciao Fault

The Ciao Ciao Fault is the largest fault zone at Passo Moro. The fault has a mean orientation of 133/77 N (Fig. 2) and was mapped for 800 m along strike but neither fault tip was observed. Based on remote sensing data (Bistacchi et al., 2000) and analysis of aerial photographs the estimated length is 8 km. The area mapped is approximately at the centre of the fault trace. The Ciao Ciao Fault trace is typically a ~15–25 m wide, talus- or snow-filled gulley with locally exposed fault rocks indicating limited variability in the architecture along strike (Fig. 1). The fault zone is composed of a zone of highly fractured bleached rock bounded by two sub-parallel, approximately planar faults (Fig. 3C). The mean fracture orientation in the central area is 138/76 N and the fracture density is ca. 20/m. Fractures in this central area are chlorite-coated and slickenlines indicate strike-slip motion (plunging 9° towards 143°). The bounding faults are characterised by a curviplanar principal slip surface embedded within the fault core. Locally two slip surfaces can be identified: one between the damage zone and breccia; and another between breccia and the fault core (Fig. 3C). Both slip surfaces are sharp, planar, polished and coated with chlorite.

The fault core is composed of breccia, cataclasite and foliated cataclasite. The breccia is pale green, lacks a fabric and is composed of 0.2–2 cm angular clasts. The cataclasite and foliated cataclasite are pale green with smears of red/brown clay-like material and are composed of matrix-supported angular 1–10 mm fragments. Within the foliated cataclasite the foliation is oriented ~146/88 N and there is a spacing of 5 mm between planes. Average density for the foliation-parallel 010 joint set varies from a maximum of 11.2/m in the metasedimentary unit to between 2.0 and 7.7/m in the augen gneisses cut by the Ciao Ciao Fault. Other joint sets that cross the fault are an order of magnitude less abundant.

The damage zone on both margins of the Ciao Ciao Fault varies from 0.4 to 3.5 m wide (Fig. 1A) and is characterised by high-density fracturing and incipient retrograde alteration. No chlorite-coated surfaces are present in the damage zone of the fault. Fracture density increases towards the fault core but the boundary between the damage zone and fault core is sharp.

4. Petrography and microstructures

All polished sections were cut perpendicular to the orientation of the fault plane and parallel to the slip direction. Analysis was carried out using a petrographic microscope, and a scanning electron microscope (Sigma SEM with integrated Oxford Instruments and INCA microanalysis computer software).

4.1. Host rocks

The granitic gneiss is the dominant host rock and the only one examined in detail. The gneiss is coarse grained with a matrix of up to 3 mm and K-feldspar augen up to 4 × 3 cm. It contains 26% quartz; 41% albite; 13% K-feldspar; 8% muscovite (Fig. 4) with 6% red-brown biotite; 1% garnet; 2% epidote; and 3% chlorite. The primary structure is the foliation, defined by biotite and muscovite. Quartz may have undulose extinction and fractures; and bulging recrystallization (Stipp et al., 2002) characterised by small recrystallized grains and bulges along the grain boundaries. Isolated primary fluid inclusions (20–30 μm) are present within quartz with rare secondary fluid inclusions (~20 μm) that form in fault parallel arrays. Subhedral K-feldspar and albite (10–500 μm) occurs within the matrix and the albite typically contains inclusions of muscovite and quartz. Garnet is anhedral and associated with chlorite and epidote.

4.2. Fault rocks

Mineral proportions and grain sizes were measured perpendicular to the principal slip surface from host rock to damage zone to fault core (Figs. 4 and 5). The damage zone of the Virgin Fault was sub-

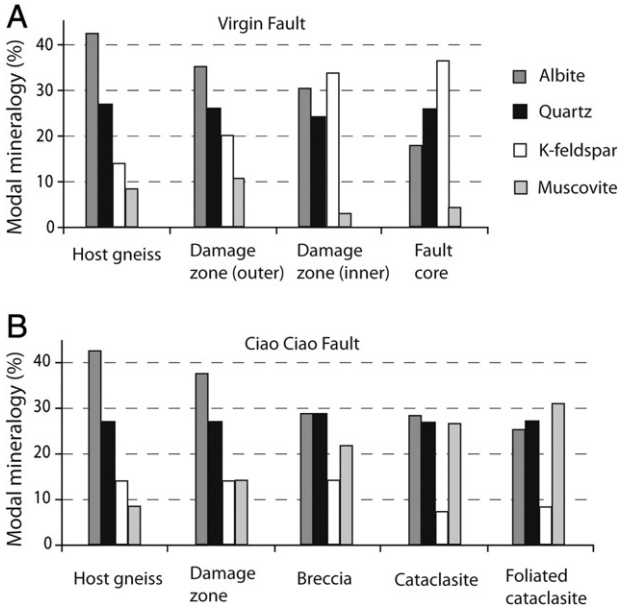

Fig. 4. Modal mineralogy of the various fault rocks of the (A) Virgin and (B) Ciao Ciao Faults. Percentages are based on point counting with estimated errors of ±3%. Minor amounts of garnet, chlorite and epidote are also present in some lithologies.

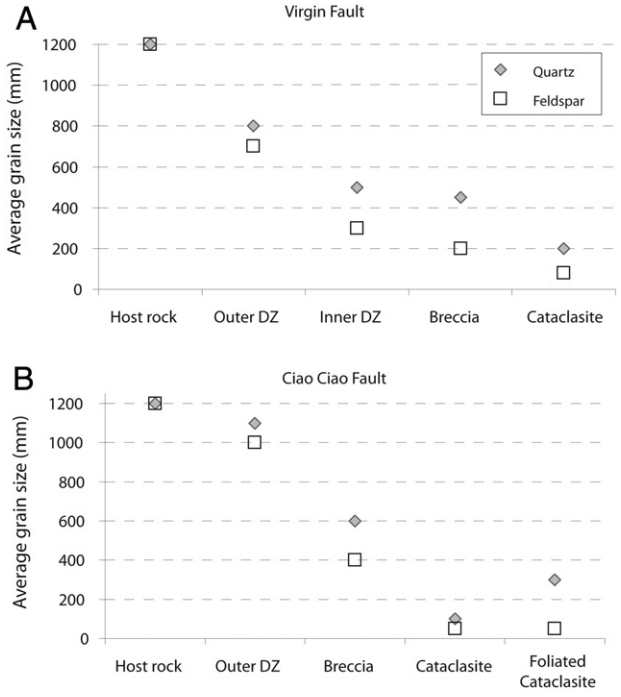

Fig. 5. Plots showing average grain size variation for matrix quartz and feldspar (both plagioclase and K-feldspar) across different structural zones of the (A) Virgin and (B) Ciao Ciao Faults.

divided into outer and inner damage zones, distinguished by variation in the intensity of bleaching, with the most intense being adjacent to the fault core. The average grain size for all minerals decreases from ~1200 μm in the host rock to ~100 μm and ~30 μm in the fault core for the Virgin Fault and Ciao Ciao Fault respectively (Fig. 5). The fault core of both the faults is dominated by 10–100 μm sized fragments however large individual clasts up to 1 mm are present throughout.

4.2.1. Virgin Fault

K-feldspar, chlorite and epidote are more abundant in the fault core than in the host gneisses, whereas albite, muscovite, biotite and garnet are less abundant. The difference in the proportions of the two feldspars is marked (Fig. 4A) with granoblastic K-feldspar dominant in the inner damage zone (Fig. 6G). Larger K-feldspars are often cut by thin veins of non-luminescent K-feldspar within the damage zone (Fig. 6G).

The outer damage zone retains most of the host rock characteristics such as a foliation, and K-feldspar augen, however within the inner damage zone the foliation is not as well defined (Fig. 6F). Bulging recrystallization is common on quartz grain boundaries throughout (Fig. 6A). Deformation is typically localised in thin anastomosing zones of fine grained quartz that initially develops along the margins of quartz subgrains in a core-mantle microstructure (Fig. 6C, D). Primary fluid inclusions in quartz within the damage zone are small (~10 μm). Albite and K-feldspar typically retain host characteristics but are subhedral (Fig. 6F), with irregular grain boundaries, and ca. 500 μm smaller than in the host (Fig. 5A). In the outer damage zone, albite is the dominant feldspar in the matrix and sparse anhedral K-feldspar tends to enclose albite. In the inner damage zone K-feldspar is the dominant feldspar in the matrix. Red-brown biotite is evenly distributed throughout the damage zone and is partially altered to chlorite. Chlorite and sparse epidote are randomly distributed throughout the matrix. No garnet is observed within the damage zone. Quartz also occurs in NW-SE trending, ~1.5 mm wide and ~5 mm long micro-veins that are typically spaced ~2 mm apart. This quartz is fractured (N-S), with undulose extinction (Fig. 6A), and contains primary isolated (up to ~70 μm) and trails of secondary (<20 μm) fluid inclusions. Chlorite (Fig. 6B) and epidote veins are oriented E-W and NW-SE with a similar orientation to the quartz micro-veins. Chlorite veins are often associated with the anastomosing zones of fine grained quartz (Fig. 6D). Epidote veins are up to 2 mm wide and 3 cm long and usually occur along the edges of quartz micro-veins. The epidote veins oriented E-W are thicker than those oriented NW-SE (500 μm compared to 100 μm), and the former are typically located closer to the boundary with the fault core.

The fault core is composed of varying amounts of breccia and/or cataclasite (Fig. 3). The breccia has dilated grain boundaries (which are often stained orange/brown); sub-grains in quartz; and chlorite veins some of which are sheared. Quartz in the fault core has more bulging recrystallization (Fig. 6B) compared to quartz in the damage zone, and contains abundant sub-grains that are oriented NW-SE. Two varieties of chlorite co-exist within the breccia (e.g. VF3) with brown/gold and purple/blue interference colours. These chlorites occur in both sheared (Fig. 6D, E) and unsheared veins (Fig. 6B). The cataclasite is composed of μm to mm clasts of quartz, K-feldspar, albite, chlorite and epidote. No recognisable host rock textures are preserved. Bands of dark grey ultracataclasite cut the cataclasite and are composed of clasts of <50 μm within a finely comminuted matrix. The clasts are quartz, albite and K-feldspar, and the matrix is primarily granoblastic K-feldspar (Fig. 6H). Numerous anastomosing thin (20 μm) sheared chlorite veins occur throughout the ultracataclasite.

4.2.2. Ciao Ciao Fault

The fault core of the Ciao Ciao Fault contains much less albite than the host gneiss and correspondingly more muscovite, from 8% in the host rock to 31% in the core (Fig. 4B).

The damage zone is characterised by K-feldspar augen, a red-brown biotite- and muscovite-defined foliation, undulose extinction and minor bulging recrystallization of quartz (similar to host), and an albite-rich matrix. Large fractures, chlorite veins and minor sericitization of feldspars are present. Fractures vary from being open, ~1 mm wide, several centimetres long and lined with muscovite (Fig. 6I) to rarer intra-crystalline closed fractures with no fill. The large open fractures are typically oriented E-W or NE-SW and spaced 1–5 cm apart, while the closed fractures typically occur in quartz and are oriented N-S. Chlorite veins are ~100 μm thick, several millimetres long, several centimetres apart and their orientations vary slightly along strike. Chlorite has blue/grey interference colours. The majority of feldspars in the damage zone are large, euhedral and sericitized within the outer 20–50 μm of the grain.

Breccia occurs between the damage zone and cataclasite (Fig. 3C) and the boundaries between the different rock types are sharp (Fig. 6J). Quartz tends to be larger (600–800 μm) than the feldspars (200–400 μm) (Fig. 5B). The breccia is dominated by fractures up to several centimetres long that are oriented NW-SE and NE-SW, with the former being more pervasive. Along the former there are often small offsets (up to 100 μm) and/or bands of recrystallization and/or brittle fragmentation of the surrounding crystals. Quartz is subhedral and randomly distributed throughout the matrix. Quartz has undulose extinction, is fractured and shows minor bulging recrystallization. Feldspars are subhedral with lobate to gently curving grain boundaries. Feldspars are often associated with muscovite that occurs around and within the outer rim of the feldspars. Muscovite also occurs in thin anastomosing bands or in large sheared clumps. Chlorite is randomly distributed throughout the breccia.

The cataclasite within the Ciao Ciao Fault is similar to that in the core of the Virgin Fault. However, no chlorite veins cut the cataclasite and there is a higher proportion of muscovite (Fig. 4B); the average grain size is smaller; and different generations of ultracataclasite are present. Ultracataclasite is composed of angular and subrounded ≤30 μm clasts of quartz, K-feldspar and albite. The different generations of ultracataclasite are distinguished by colour and the

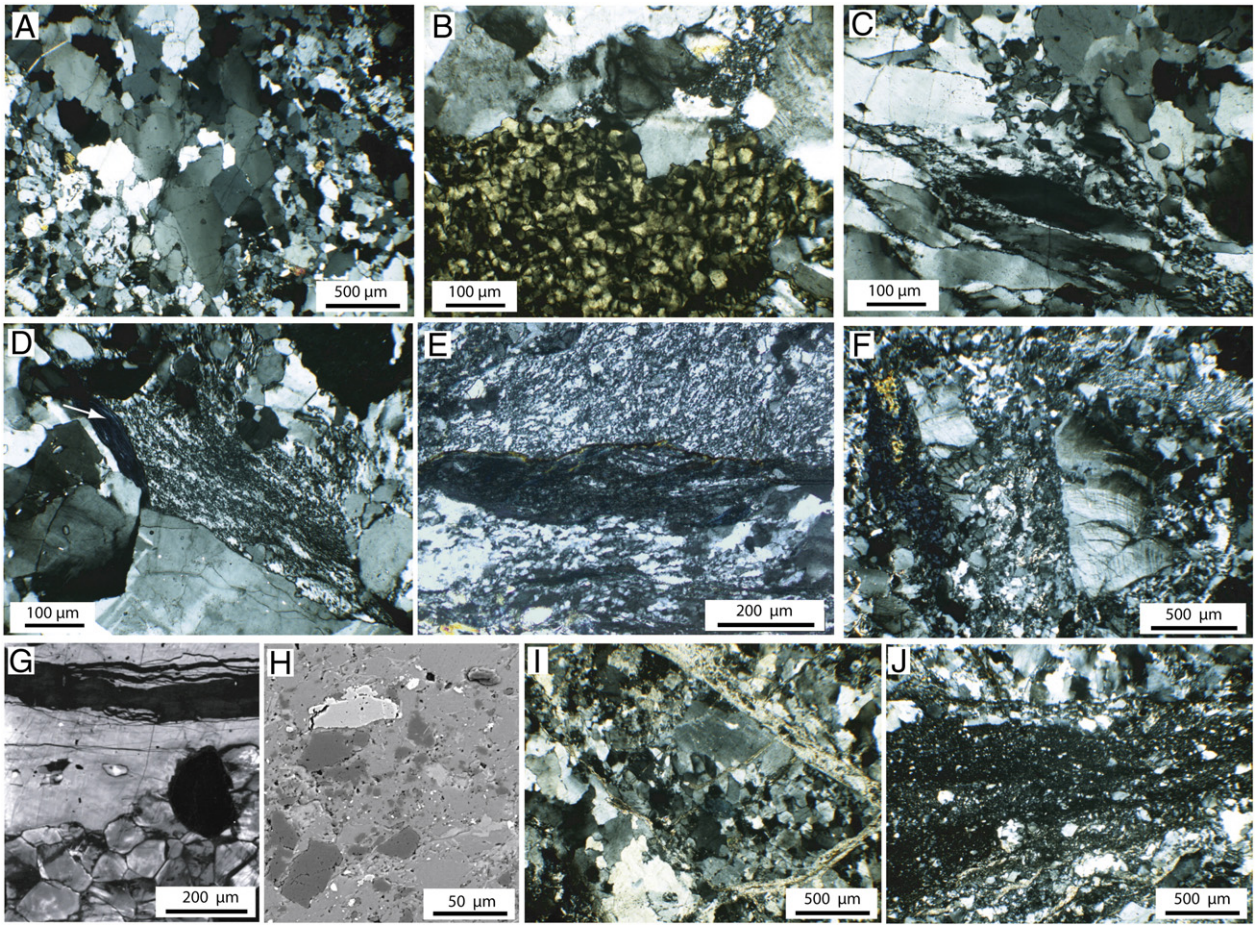

Fig. 6. Representative thin section microtextures of fault zone rocks, crossed polarized images unless stated otherwise. A) Coarsely crystalline thin quartz microveins with bulging recrystallization on grain boundaries and subgrains (central area) (VF5, outer damage zone); B) Unsheared chlorite vein (lower half of image) (VF2, fault core); C) Strongly deformed quartz showing core and mantle texture, with fine grained recrystallised quartz on grain boundaries and along zone oriented top right to lower left (VF21, outer damage zone); D) Deformed zone of finely recrystallised quartz with margin of sheared chlorite (arrowed) (VF21, outer damage zone); E) Sheared chlorite vein surrounded by quartz recrystallised by bulging recrystallization (VF2, fault core); F) Fractured K-feldspar porphyroclast, in fine grained recrystallised quartz and feldspar with unsheared chlorite vein (right side of image) (VF17, inner damage zone); G) Cathodoluminescence image of K-feldspar porphyroclast with recrystallised granoblastic K-feldspar at margins and vein of non-luminescent K-feldspar (VF6, inner damage zone); H) Backscattered electron image of K-feldspar cemented (medium grey) cataclasite with clasts of epidote (bright grey), quartz and albite (dark grey) (VF2, fault core); I) Muscovite veins and foliation planes through feldspar-rich matrix and adjacent quartz microvein with bulging recrystallization (right side of image) (CC3, foliated cataclasite); J) Ultracataclasite (centre) at boundary between breccia and cataclasite (CC2).

proportion of clasts to comminuted material. Boundaries between the ultracataclasites are sharp. At the boundary between the breccia and the cataclasite there is a thin injection vein of brown/black ultrafine clasts (<20 μm), associated with a thin ultracataclasite (Fig. 6J). Muscovite and chlorite are fine grained (~50–200 μm) throughout the cataclasite and evenly distributed. They often align in undulating thin bands oriented NW-SE and are associated with fracture planes. Quartz and feldspar have similar textures to those in the cataclasite from the Virgin Fault, although both are finer grained (~20–40 μm) (Fig. 5B). A few strongly sericitised 110 μm feldspar clasts are present with larger (up to 150 μm), angular quartz clasts.

The foliated cataclasite is similar to the cataclasite, with an anastomosing foliation defined by thin muscovite-rich bands (Fig. 6I). However in the former, muscovite proportions are higher, albite is less abundant (Fig. 4B) and there are no cross-cutting ultracataclasites. Chlorite veins vary in thickness along their trace (10s of μm to 100 s of μm). Quartz micro-veins (1–3 mm long) within the foliated cataclasite are oriented approximately NW-SE, sub-parallel to the foliation, and contain coarse (200–500 μm) quartz (Fig. 6I). Some micro-veins have undeformed quartz, whereas other micro-veins contain fractured quartz with undulose extinction.

5. Fluid–rock reactions and conditions of faulting

5.1. Virgin Fault

In the Virgin Fault the foliation from the host rock is progressively broken down towards the cataclasite accompanied by the loss of biotite and muscovite. The breakdown of micas to produce chlorite is associated with the generation of quartz and K^+ in the fluid (Reaction 1).

$$\text{Biotite} + \text{Muscovite} + \text{Water} = \text{Chlorite} + \text{Quartz} + K^+ \quad \text{(Reaction 1)}$$

However the overall proportion of quartz does not change from host rock to cataclasite. Hence the precipitation of quartz in micro-veins may reflect a closed system involving dissolution of quartz from the matrix. The major decrease in the abundance of albite is matched by an increase in K-feldspar in the fault core (Fig. 4A). This reaction (Reaction 2) can occur in a closed system in response to changing temperature and pressure conditions, however this typically only causes limited volumes of reaction (Wintsch, 1975).

$$\text{Albite} + K^+ = \text{K-feldspar} + Na^+ \quad \text{(Reaction 2)}$$

In an open system, introduction of K^+ or loss of H^+ enables larger volumes of K-feldspar to precipitate. Therefore feldspathization in the Virgin Fault was associated with infiltration of fluids into the fault zone and near neutral pH conditions (Wintsch et al., 1995). The cataclasite is composed of clasts of quartz, albite, K-feldspar and epidote set in an undeformed K-feldspar-rich cement (Fig. 6C) precipitated from a K^+-rich fluid. Chlorite veins cut the cataclasite indicating that cementation of this fault rock prevented cataclastic flow and promoted brittle fracturing.

Bulging recrystallization and undulose extinction in the quartz micro-veins indicate that ambient temperatures were ~300 °C. The temperature did not exceed 350 °C because sub-grain rotation did not occur (Stipp et al., 2002). Bulging recrystallisation is typically restricted to grain boundaries, however adjacent to sheared chlorite veins and the principal slip surface, quartz is completely recrystallized. Locally variable amounts of bulging recrystallization on a mm-scale associated with the principal slip surface and sheared veins may reflect localised high strain rates (Hirth and Tullis, 1992). Chlorite and epidote veins in the Virgin Fault also indicate temperatures <350 °C during fluid infiltration (Bird and Spieler, 2004) and the presence of both sheared and unsheared chlorite veins, suggests at least two phases of chlorite veining separated by a phase of deformation.

5.2. Ciao Ciao Fault

The main change occurring from host rock to fault core of the Ciao Ciao Fault is the decrease in feldspar abundance and an increase in muscovite (Fig. 4B). This is a result of sericitization of albite and/or K-feldspar (Reactions 3 and 4) and indicates the presence of a low pH fluid (Wintsch et al., 1995).

$$\text{K-feldspar} + H^+ = \text{Muscovite} + K^+ + \text{Quartz} \quad \text{(Reaction 3)}$$

$$\text{Albite} + K^+ + H^+ = \text{Muscovite} + Na^+ + \text{Quartz} \quad \text{(Reaction 4)}$$

To create such conditions, fluids must have been abundant, as smaller amounts of fluid result in K-feldspar precipitation (Wintsch, 1975). However there is no evidence for quartz precipitation associated with sericitization in the damage zone, breccia or cataclasite. Open system behaviour promotes quartz dissolution and retrograde alteration of feldspar creating porosity (Janssen et al., 1998; O'Hara, 2007). So quartz may remain in solution and be removed from the fault zone. However, quartz within the matrix does not show dissolution textures and this, combined with the incomplete nature of the sericitization reaction, indicates that the open system conditions were short-lived. The Ciao Ciao Fault also preserves minor bulging recrystallization in quartz, fracturing and cataclasis, and chlorite veining; these features indicate that the temperature was <350 °C.

The grain size of quartz is greater in the foliated cataclasite (Fig. 5B) than in its probable precursor, the cataclasite which may indicate a phase of quartz precipitation. Quartz micro-veins vary from being undeformed to those with undulose extinction and fractures. Such textures are likely to be the result of several micro-veining events. Hence quartz precipitated periodically within the foliated cataclasite during faulting, and as the fault core evolved it ceased to be an open system and became a barrier type system. The foliation defined by muscovite, produced in response to retrogression of feldspars, may have acted as a fluid seal, lowered permeability and locally promoted quartz precipitation (Janssen et al., 1998).

Microstructures indicate that the Ciao Ciao Fault deformed by cataclastic flow with limited to no plastic deformation (cf. Hirth and Tullis, 1994), in contrast, the Virgin Fault deformed predominantly by semi-brittle flow involving cataclasis and crystal plastic behaviour. These differences indicate that the Ciao Ciao Fault deformed at ca. 250 °C under brittle conditions while the Virgin Fault deformed at slightly higher temperatures (ca. 300 °C). Such conditions of metamorphism are compatible with muscovite being the dominant "white phyllosilicate" present in the fault rocks, although illite may be formed in some of the lower temperature feldspar replacement reactions (Verdel et al., 2011).

6. Fluid inclusions

Fluid inclusion analysis was carried out on double-polished fluid inclusion wafers using a Linkham THMSG600 heating-freezing stage mounted on a Zeiss Axioplan microscope. Microthermometric studies were carried out using standard procedures (e.g. Shepherd et al., 1985).

The majority of fluid inclusions in the host gneiss are two phase, liquid-vapour with 90–95% liquid fill. The remainder are purely liquid (no vapour bubble), purely vapour, or liquid-vapour + CO_2. Within the faults, the quartz micro-veins contain large (>25 μm) primary inclusions, while recrystallised quartz has very small inclusions. The Ciao Ciao Fault has a greater number of fluid inclusions than the Virgin Fault, although only the fluid inclusions in the latter were large enough to analyse.

Homogenization temperatures for primary inclusions in the cataclasite and inner damage zone of the Virgin Fault range from 180 °C to 230 °C (Table 1). A quartz-filled joint oriented 090/90 with both primary and secondary inclusions was analysed (Table 1) and has homogenization temperatures of 296 °C and 187 °C respectively. The primary fluid inclusions show no phase transitions on heating, so there is no evidence for CO_2 in the fluids. Within the fault, the temperature of first melting of the aqueous phase (Tfm) varies from −28 to −10 °C and the temperature when the aqueous phase became ice-free (TmIce) was from −4 to 0 °C which implies that the fluid is of low salinity with 0–6.45 wt% equivalent NaCl (Sheppard, 1986; Bodnar, 1993). At Monte Rosa, Curti (1987) estimated that the pressure

Table 1
Heating/freezing data fromfluid inclusions. Locations for Virgin Fault samples shown in Fig. 1B, Qtz1 is a quartz veinwith 090 orientation in the host gneisses that predates faulting.VF14 is a sample of cataclasite, VF12 is a vein in the inner damage zone.

Sample	Inc. No	Liquid fill (%)	P or S	Size (μm)	Tfm (°C)	TmIce (°C)	T_H (°C)	Trapping temp (°C)$^+$	Trapping temp (°C)$^{++}$
VF14	1	90	P	45	−28	−4	230	270	380
	2	95	P	40		0			
	3	95	P	25		−0.1	180	210	310
	4	90	P	40	−10	−1.8	180	210	310
VF12	1	90	P	25	−27.9	−3.6	200	230	320
	2	95	P	20			210		
Qz1	1	95	P	25		−5.3	296	370	470
	2	95	S	20			185		
	3	95	S	25			188		
Average							196 °C		

P = primary inclusion; S = secondary inclusion.
$^+$ Trapping temperature uses the homogenization temperature and estimated minimum pressure (Curti, 1987), and isochores constructed by Bodnar and Vityk (1994).
$^{++}$ Trapping temperature uses estimated maximum pressure (Curti, 1987).

was 1.7–2.2 kb and fluid pressure was 0.8–1.4 kb. Corrected temperatures, calculated for the minimum fluid pressure and maximum lithostatic pressure using isochores constructed by Bodnar and Vityk (1994) (Table 1), provide an estimate of the minimum and maximum trapping temperature of fault zone fluids to be 210 °C and 380 °C respectively.

7. Stable isotopes

Stable isotopic compositions of the minerals in the host gneisses and fault rocks were determined to assess the origin of the hydrothermal fluids. In-situ micro-sampling, using the New Wave Micromilling system, yielded ca. 1 mg of powder of specific minerals for O analyses. Separates were analysed for O isotopes using a laser fluorination procedure, involving total sample reaction with excess ClF_3 using a CO_2 laser at temperatures in excess of 1500 °C (Sharp, 1990). All fluorinations resulted in 100% release of O_2 from the silicate lattice. This O_2 was converted to CO_2 by reaction with hot graphite, and analysed by a VG SIRA 10 spectrometer. Data were discarded for samples producing either unrealistically high or low yields (Lawther, 2011). Results are reported in standard notation ($\delta^{18}O$) as per mil (‰) deviations from Vienna Standard Mean Ocean Water (V-SMOW).

Mineral separates were prepared for H analysis using conventional separation techniques. Quartz separates were obtained using LST Fastfloat® and froth flotation. All separates were examined by binocular microscope to ensure purity. Hydrogen analysis was done by *in vacuo* bulk heating. 1 g of quartz and K-feldspar, and 0.05 g of phyllosilicate were analysed using the method of Donnelly et al. (2001) and a VG-Micromass 602D mass spectrometer (Lawther, 2011). Results are reported in standard notation (δD) as per mil (‰) deviations from Vienna Standard Mean Ocean Water (V-SMOW). δD results for quartz and K-feldspar represent the composition of fluid inclusions whereas the water released from chlorite, epidote and muscovite is structural. The coincidence of similar low yields of water from quartz (0.06 ± 0.04 μmol/mg) and feldspar (0.08 ± 0.05 μmol/mg), and the lack of statistical correlation of yield versus δD of included fluids indicates that micro-alteration of K-feldspar was likely trivial, and did not add significantly to the water budget from the pyrolysis.

7.1. Host rock results

7.1.1. Oxygen isotopes

Quartz has an average $\delta^{18}O$ value of 12.3 ± 0.3‰ and K-feldspar a value of 9.5‰ (Fig. 7). Equilibrium $\delta^{18}O_{Fluid}$ values calculated using fractionation equations (O'Neil and Taylor, 1967; Matsuhisa et al., 1979) yield a range from 8.4 to 9.8‰ for quartz and 7.3‰ for K-feldspar. $\delta^{18}O_{mineral}$ results from Frey et al. (1976) for quartz and K-feldspar were 12.5‰ and 10.4‰ respectively.

7.1.2. Hydrogen isotopes

The δD_{Fluid} value of muscovite is −46‰ and a range of −99 to −129‰ was measured for quartz and K-feldspar, using the fractionation equation of Suzuoki and Epstein (1976). The equivalent host rock data of Frey et al. (1976) converts to a δD_{Fluid} range of −15 to −35‰. Muscovite from this study falls outside this range, while quartz and K-feldspar have isotopic values consistent with interaction with meteoric water-like fluids. Frey et al. (1976) recorded three 'abnormal' results from biotite and phengite which when converted indicate δD_{Fluid} values around −80 and −140‰ (estimated from Bowers and Taylor, 1985). Therefore quartz and K-feldspar results from this study corroborate with Frey et al. (1976) confirming evidence for interaction of a deuterium-depleted meteoric fluid with the host rock, subsequent to initial deposition.

7.2. Fault rocks

7.2.1. Oxygen Isotopes

$\delta^{18}O$ values of quartz, K-feldspar and chlorite from both fault zones are tightly clustered (Fig. 7) (Table 2) and imply there was a common hydrologic regime (Baker, 1990). Quartz $\delta^{18}O$ values from the Virgin Fault are almost identical to the host but in the Ciao Ciao Fault they

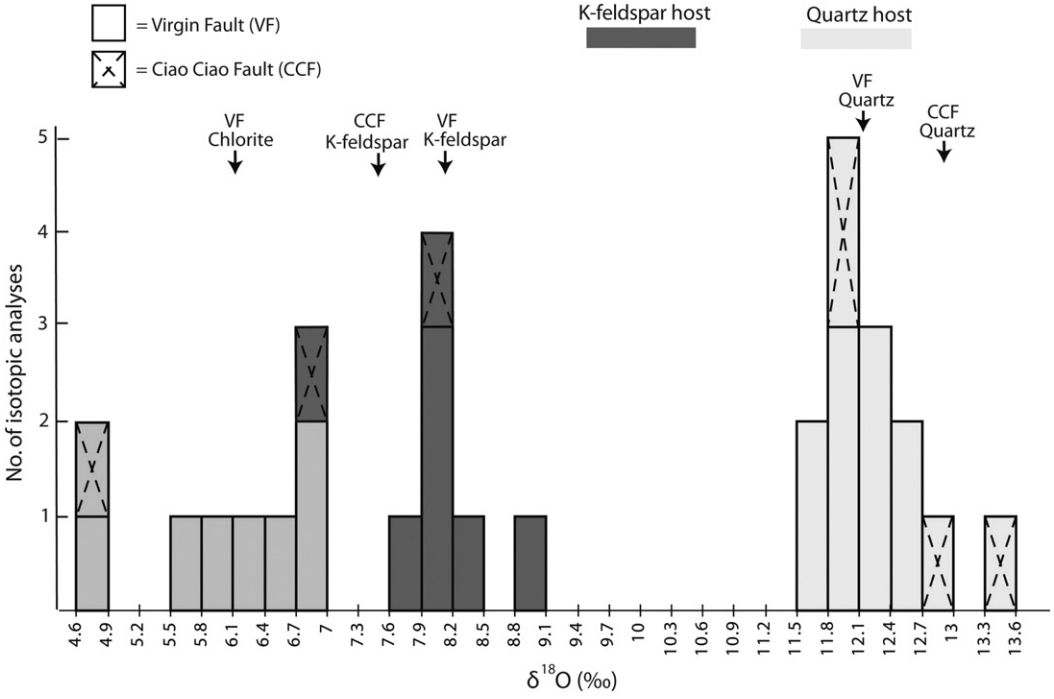

Fig. 7. Histogram showing $\delta^{18}O$ values of fault rock minerals from the Virgin and Ciao Ciao Faults. The range of host rock values for quartz and K-feldspar are also shown with the latter incorporating a $\delta^{18}O$ analysis from Frey et al. (1976). The mean $\delta^{18}O$ value for each mineral in each fault is indicated. Analyses of K-feldspar shown in dark grey; quartz in pale grey and chlorite in intermediate shade grey.

are slightly higher than the host (Fig. 7). In both faults, K-feldspar is depleted in ^{18}O with respect to the host rock, but is most depleted in the Ciao Ciao Fault. Chlorite from both fault zones records the lightest $\delta^{18}O$ values of all the minerals (Fig. 7). Quartz $\delta^{18}O$ composition increases from the outer damage zone of the Ciao Ciao Fault through to the fault core (Table 2). The damage zone and breccia have almost identical $\delta^{18}O$ signatures but the $\delta^{18}O$ is ~2‰ higher in the foliated cataclasite compared to host.

Table 2
Oxygen and hydrogen stable isotope data for all samples. Sample locations are shown in Fig. 1B for the Virgin Fault (sample prefix VF). For the Ciao Ciao Fault (sample prefix CC) (Fig. 1A), location of sample (5) is marked as c, sample (24) is from the SE extremity of mapped trace of the fault, and (Amph) is from the amphibolite to the north of the fault trace in Fig. 1A. For oxygen analyses the standards used were NBS-28 (quartz sand), SES (quartz), UWG-2 (garnet) with results having an average uncertainty of ± 0.1‰ and standard deviation of 0.3‰. The standards used during hydrogen analyses were v-SMOW, GISP and Lt Std with results having an average uncertainty of ± 3‰ and standard deviation of 1.1‰. It is assumed that the uncertainty associated with the standards is the same as for the mineral samples.

Sample[1]	Rock type	Mineral	$\delta^{18}O$ (‰)	$\delta^{18}O_{Fluid}$(‰)[a]	δD_{Fluid}(‰)[b]
Host 1	AG	Qz	12.7	9.6	−99
Host 1	AG	Kfs	9.5	7.3	−101
Host 3	AG	Qz	11.7	8.7	−125
Host 3	AG	Kfs			−129
Host 3	AG	Musc			−46
Host 4	AG	Qz	12.7	9.6	
Mean Qz value			**12.3 ± 0.6**	**9.3 ± 0.5**	
VF1	ODZ	Qz			−119
VF2	FC	Qz	12.1	0.5	−83
VF2	FC	Qz	12.2	0.6	−83
VF3	FC	Qz	12.5	0.8	−119
VF4	FC	Qz	11.8	0.2	
VF5	OCZ	Qz	12.1	0.5	
VF6	IDZ	Qz	11.6	0	
VF7	FC	Qz	12.4	0.7	−107
VF8	ODZ	Qz	11.7	0.1	−119
VF12	IDZ	Qz	12.4	0.7	−78
VF14	FC	Qz	12.2	2.3	−82
Mean value			**12.1 ± 0.3**	**0.7 ± 0.7**	**−99 ± 18.9**
CC1 (5)	DZ	Qz	11.9	0.3	
CC2 (5)	FC	Qz	12.1	0.5	
CC3 (5)	FC	Qz	14.1	2.5	−120
CC3 (5)(repeat)	FC	Qz	13.4	1.8	−120
CC4 (24)	DZ	Qz	12.9	1.3	−122
Mean value			**12.9 ± 0.9**	**1.3 ± 0.9**	**−121 ± 1.4**
VF1	ODZ	Kfs			−135
VF2	FC	Kfs	8	−1.6	−99
VF3	FC	Kfs	8.4	−1.2	−95
VF5	ODZ	Kfs	8	−1.6	
VF7	FC	Kfs	7.6	−2	−113
VF8	ODZ	Kfs	8.8	−0.8	−134
VF14	FC	Kfs	8.1	−0.1	−69
Mean value			**8.1 ± 0.4**	**−1.2 ± 0.7**	**108 ± 25.3**
CC3 (5)	FC	Kfs	6.8	−2.8	−129
CC4 (24)	DZ	Kfs	8.2	−1.4	−114
Mean value			**7.5 ± 1.0**	**−2.1 ± 1.0**	**−122 ± 10.6**
VF2	FC	Chl	6.9	3.5	−32
VF3	FC	Chl	6.7	3.3	−18
VF5	ODZ	Chl	5.8	2.5	
VF7	FC	Chl	5.7	2.3	−19
VF8	ODZ	Chl	6.6	3.3	−29
VF12	IDZ	Chl	4.6	1.2	−17
VF14	FC	Chl	6.2	0.1	−30
Mean value			**6.1 ± 0.8**	**2.3 ± 1.3**	**−24 ± 6.9**
CC3 (5)	FC	Chl			−79
CC4 (24)	DZ	Chl	4.7	1.3	−65
Mean value					**−72 ± 9.9**
VF3	FC	Musc			−72
VF14	FC	Musc			−109
CC (18)	Amp	Musc			−46

FC = fault core, ODZ = outer damage zone, IDZ = inner damage zone, DZ = damage zone, AG = Augen gneiss host rock.

[a] $\delta^{18}O_{Fluid}$ calculated using the fractionation equation for the mineral together with estimated temperature of 450 °C for the host rock (Frey et al., 1976) and average fluid inclusion temperature of 196 °C for the fault rocks.

[b] δD for muscovite and chlorite calculated using the appropriate fractionation equation.

7.2.2. Interpretation—oxygen isotopes

Quartz-K-feldspar mineral pairs typically yield calculated equilibrium temperatures of −20 to +110 °C, these are thought to be unrealistic for the estimated conditions of faulting and much lower than those measured from fluid inclusions (180–230 °C). This implies that disequilibrium between quartz and K-feldspar and may indicate open system behaviour (Jenkin et al., 1992). The fault core of the Ciao Ciao Fault records the greatest degree of disequilibrium between quartz and K-feldspar, with unrealistic inferred equilibrium temperatures of −20 to +25 °C.

For each sample from the Virgin Fault, there are no realistic fluid $\delta^{18}O$ – temperature combinations where quartz, K-feldspar and chlorite are in equilibrium with the same fluid (Fig. 8A). Microstructural evidence indicates that the temperature during deformation was relatively stable (e.g. bulging recrystallization common throughout), thus using the mean fluid inclusion temperature (200 °C) implies that chlorite, quartz and K-feldspar precipitated from, or interacted with, progressively lighter fluids.

Within the Ciao Ciao Fault, quartz and chlorite could be in equilibrium with the same fluid between 160 and 230 °C and chlorite and K-feldspar could also potentially have been in equilibrium at ~110 °C (Fig. 8B). However locally chlorite veins cut K-feldspar and it is thus unlikely that these phases were in equilibrium during faulting: this resonates with the theoretical temperature for equilibration being lower than that measured for fluid inclusions and unrealistically low given the predicted conditions of faulting. Quartz micro-veins and chlorite

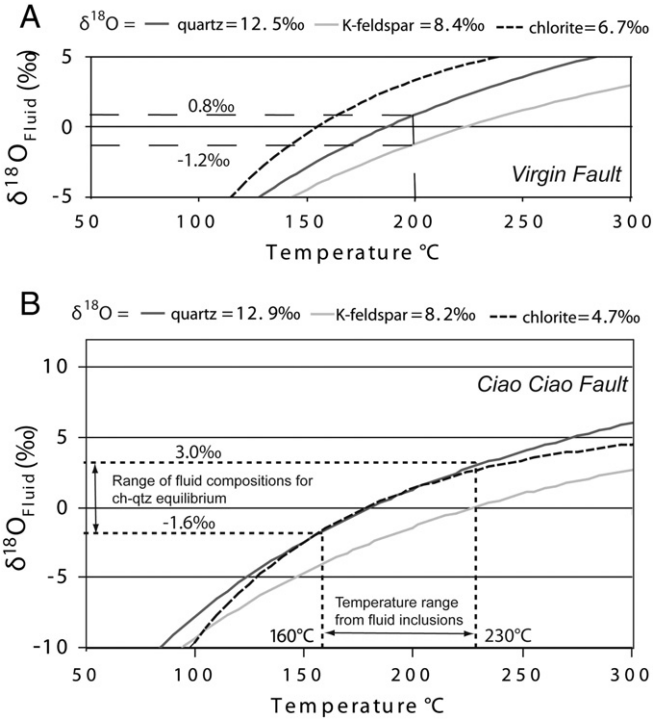

Fig. 8. Equilibrium fluid plots showing $\delta^{18}O_{Fluid}$ in equilibrium with different fault rock minerals as a function of temperature. Modelled curves intersect when co-existing minerals are in equilibrium with the same fluid at the same temperature. A) Equilibrium fluid diagram for co-existing minerals from VF3 (Virgin Fault). Different equilibrium fluid compositions are highlighted for quartz and K-feldspar at 200 °C and the plot indicates the lack of a common co-existing fluid. B) Equilibrium fluid plot for co-existing minerals from CC4 in the Ciao Ciao Fault. Dotted lines highlight the temperature range indicated by fluid inclusion thermometry and point towards the composition of a co-existing $\delta^{18}O$ fluid with which quartz and chlorite could have been in equilibrium.

veins could be co-genetic, so it is possible that quartz and chlorite equilibrated with the same fluid at 160–230 °C (Fig. 8B).

Within both faults, the K-feldspar isotopic compositions typically infer equilibration with lower $\delta^{18}O$ fluids than those for quartz and chlorite (Fig. 8). After precipitation, both quartz and chlorite are unlikely to exchange oxygen with another fluid below temperatures of ~500 °C (Giletti, 1986; Criss et al., 1987). However, K-feldspar can exchange oxygen isotopes with a fluid down to 50 °C (Wenner and Taylor, 1976). This suggests that after precipitation of the chlorite veins, the K-feldspar was isotopically re-equilibrated in the presence of another pervasive isotopically light fluid in the fault zone. Consequently based on a combination of isotopic and textural evidence in the Virgin Fault, there were probably a minimum of four fluids, the first precipitated quartz and possibly K-feldspar; the second precipitated some of the chlorite veins, the third precipitated the second set of chlorite veins and the fourth reset the isotopic composition of K-feldspar. In the Ciao Ciao Fault, the first fluid precipitated quartz and chlorite, the second precipitated the second generation of chlorite veins and the third reset the oxygen isotopes of the K-feldspar.

The $\delta^{18}O$ value of the damage zone quartz in the Ciao Ciao Fault is identical to that of the host rock. There is no evidence for newly precipitated quartz in the damage zone and quartz is unlikely to re-equilibrate at low temperatures (Gilleti, 1986), thus it will retain the host rock signature. Although fluid–rock interactions can typically result in a significant reduction in the $\delta^{18}O$ signature of the rock (Sheppard, 1986), the foliated cataclasite has a higher $\delta^{18}O$. At low temperatures, the $\delta^{18}O$ can be increased through interaction between rocks and meteoric waters, if permeability was low (Criss and Taylor, 1986). Cataclasite formation due to repeated slip events and foliation development will progressively reduce permeability (Jefferies et al., 2006a) and decrease the water–rock ratios. Hence the high $\delta^{18}O$ of the foliated cataclasite may confirm the textural evidence that the fault ceased to be an open system and was no longer being refreshed by external fluids.

7.2.3. Hydrogen isotopes

The δD_{Fluid} compositions for the faults range from −17 to −135‰ (Table 2) with two groups of data. A heavier group (−15 to −35‰) is derived from chlorite from the Virgin Fault and is within the range of fluid compositions estimated for the unmodified host gneiss (Frey et al., 1976). Other samples including chlorite from the Ciao Ciao Fault are part of a lighter group (−65 to −135‰) (Table 2). To attain such light values the minerals in both faults must have interacted with a deuterium-depleted meteoric fluid.

7.2.4. Interpretation—hydrogen isotopes

Chlorite is the only mineral from the Virgin Fault that records a host-rock like δD_{Fluid} signature. Hydrogen exchange in chlorite is slow below 500 °C (Graham et al., 1987) and δD is unlikely to be reset after growth of chlorite in the fault rocks. However, hydrogen exchange rates are rapid for muscovite between 150 and 400 °C (Vennemann and O'Neil, 1996), explaining how co-existing muscovite and chlorite can have significantly different δD_{Fluid} values. Fluid inclusions will dominate the δD signature of quartz and K-feldspar (Gleeson et al., 2008) and consequently their isotopic compositions can also potentially be modified (Burgess et al., 1992). Microstructural observations reveal that quartz and K-feldspar precipitated prior to chlorite, and presumably formed from a similar fluid to that which precipitated chlorite. Undeformed chlorite is texturally associated with isotopically lighter quartz, which implies that there were periodic influxes of isotopically lighter fluids into the Virgin Fault without significant subsequent deformation. Isotopic results from the Virgin Fault therefore indicate that during exhumation, the fault rocks may have interacted with increasingly meteoric-like fluids with a δD_{Fluid} of −135‰. However, microstructures and isotopic composition of chlorite show that most mineralization and deformation in the fault were likely in equilibrium with deeper, metamorphic fluids. Given the concordance of the chlorite results with those of Frey et al. (1976), it is possible that the original fault zone fluids were the same as those in which Monte Rosa 'stewed'.

Chlorite records δD_{Fluid} values of −65 to −80‰ within the Ciao Ciao Fault whereas quartz and K-feldspar record values between −110 and −130‰ (Table 2). These values are outwith the range of fluid compositions determined for the host gneiss and imply that the fault only records interaction with lighter fluids. Since chlorite is unlikely to be isotopically modified, the relatively heavy isotopic compositions may represent an early, rock-buffered fluid of mixed origin that was present during fault growth. Quartz and K-feldspar isotopic compositions within the fault core indicate that meteoric fluids were involved during exhumation.

Excluding chlorite, because of its propensity to retain original isotopic signatures, the δD_{Fluid} values range from −69 to −134‰ and −114 to −129‰ for the Virgin Fault and Ciao Ciao Fault respectively. Hence, the Virgin Fault records a greater range of δD_{Fluid} composition, than the Ciao Ciao Fault. Although the data set for the latter is more limited, analyses come from samples that are up to 800 m apart and so this implies there was a pervasive fluid throughout the fault zone causing widespread isotopic re-equilibration. In contrast, variation of δD_{Fluid} values within and between samples in the Virgin Fault points to the lack of a common hydrologic system in this fault.

8. Fluid variations and water-rock modelling

Fluid evolution with varying water–rock ratios and temperature can be modelled for a rock and fluid of given compositions (Criss and Taylor, 1986). In the modelling, the initial $\delta^{18}O$ composition of the rocks is given by the host rocks ($\delta^{18}O$ 12.3‰; δD −60‰). The initial δD of the hydrothermal fluid can be estimated from the chlorite isotopic composition. By applying the meteoric water equation, the initial $\delta^{18}O$ of the meteoric fluid may be calculated (Taylor, 1977), and the evolution of the hydrothermal fluid modelled for varying water–rock ratios. Results are compared to these modelled curves to indicate if samples formed in a system with an evolving water-rock ratio or from different fluids. Three initial compositions of infiltrating fluids were modelled based upon the δD_{Fluid} composition of chlorite in the Virgin Fault (~δD −25‰ (Fluid A, Fig. 9)) and the Ciao Ciao Fault (δD −65‰ (Fluid B, Fig. 9)), and from the lowest δD_{Fluid} value recorded in the Ciao Ciao

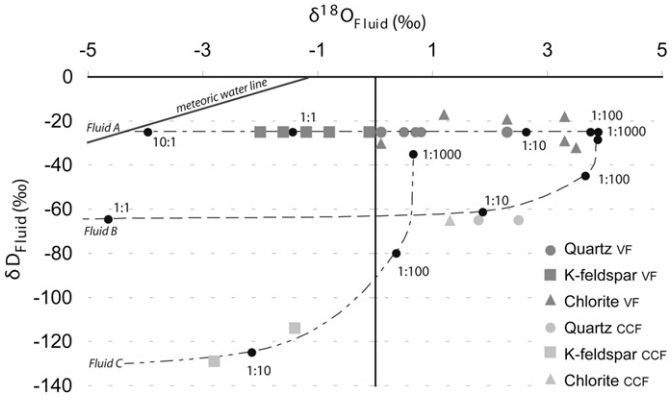

Fig. 9. $\delta^{18}O_{Fluid}/\delta D_{Fluid}$ plot showing comparison between fluid isotopic compositions calculated from modified and actual mineral isotopic data from the Virgin (VF) and Ciao Ciao Faults (CCF) with modelled curves of fluid evolution (dashed lines) based on initial fluid composition and variable water/rock ratio. Quartz and K-feldspar δD_{Fluid} values are modified to that of the co-existing chlorite in the Virgin Fault and only quartz is modified in the Ciao Ciao Fault. Three fluid compositions are used for the modelling: Fluid A—in equilibrium with chlorite from Virgin Fault; Fluid B—in equilibrium with chlorite from Ciao Ciao Fault; and Fluid C—lowest δD_{Fluid} recorded in Ciao Ciao Fault. Various water/rock ratios labelled associated with black circles along modelled curves. Modelling follows Ohmoto and Rye (1974), using initial host rock composition of $\delta^{18}O$ 12.3‰ (quartz, this study) and δD_{Fluid} −60‰ (biotite (Frey et al., 1976)).

Fault (δD −135‰ (Fluid C, Fig. 9)). Fluid inclusion temperatures provide a minimum trapping temperature of ~210–270 °C (Table 1) for the fault zone fluids. Isotopic compositions of quartz (δD) and K-feldspar (δD) from both faults indicate they interacted with a more meteoric-like fluid at ~200 °C. For water–rock modelling a fluid temperature of 260 °C was chosen for the two heavier fluids (Fluids A & B) and 200 °C for the lighter fluid (Fluid C) as these resulted in fluid evolution paths that best fitted the data.

Microstructural evidence suggests that quartz and K-feldspar may have originally formed from, or interacted with, a similar fluid to that which precipitated chlorite. Consequently, initial δD_{Fluid} values of quartz and K-feldspar were assumed to be identical to the fluid isotopic values indicated by the chlorite. Once this is adjustment is made all data points fall close to modelled fluid evolution curves (Fig. 9). Multiple curves are needed to fit the data (dictated by the variable chlorite analyses) and this reflects the presence of multiple fluids in the fault zones. However, the close proximity of the data points to the modelled fluid evolution curves indicates that the fluids in the fault zone can be assessed in terms of evolving water–rock ratios. The δD of K-feldspar was not adjusted from the Ciao Ciao Fault as the two data points do fall along the calculated fluid evolution path for a fluid with δD −135‰ (Fluid C, Fig. 9). This is the lightest fluid recorded within the faults and was the last fluid that precipitated the K-feldspar or modified its isotopic composition.

8.1. Water–rock modelling results

8.1.1. Virgin Fault

Within the Virgin Fault, the homogeneity of individual mineral $\delta^{18}O$ compositions (Fig. 7) indicates a common hydrological system, but disequilibrium between minerals implies the system was open to fluids. Water–rock ratios vary from rock-dominated (1:100) to a regime with more water present (towards 1:1) (Fig. 9, Fluid A)). Chlorite veins, formed after quartz and K-feldspar, are associated with lower water–rock ratios than quartz or K-feldspar, and thus the Virgin Fault is thought to become progressively more "rock-dominated". We interpret this to mean that during evolution of the Virgin Fault, fluids were infiltrating but also being used up and likely resulted in mineral precipitation causing cementation of the fault rock.

Quartz and K-feldspar record light δD fluids within the fault zone as a result of trapping later meteoric-like fluids (*cf.* Barker et al., 2000; Menzies et al., 2014). This implies that the Virgin Fault must have been open to fluids at a later stage. Such behaviour in faults may represent a combined conduit-barrier type system (Logan and Decker, 1994; Goddard and Evans, 1995) where brittle failure allows the infiltration of fluid and cementation seals the fault (Janssen et al., 1998). The variable δD composition of fluid recorded by quartz and K-feldspar even within an individual sample in the Virgin Fault (Table 2) indicates the influence of multiple fluids with the lack of a single pervasive fluid. This points towards the fault being a limited open system whereby finite volumes of fluid would periodically infiltrate the fault zone.

8.1.2. Ciao Ciao Fault

The data from the Ciao Ciao Fault suggest a relatively consistent water–rock ratio of ca. 1:10 (Fig. 9, Fluids B & C). Therefore, the fault records information on periodic influxes of different fluids. Within this fault, quartz records the lowest water–rock ratio (Fig. 9). This suggests that the fault was not an open system. The continued influx of fluid tends to cause silica dissolution and retrograde replacement of feldspar creating porosity (Janssen et al., 1998) as opposed to silica precipitation. Both microstructural and isotopic evidence points towards the foliated cataclasite being deformed, sealed and deformed again. Thus the foliated cataclasite of the Ciao Ciao Fault is subject to cycles of higher and lower permeability and is a limited open system for fluids.

9. Discussion

9.1. Mineralogical and mechanical controls on fault strength

Mechanical deformation is intimately linked with chemical processes and once deformation starts, and provided that there is sufficient fluid, reactions will occur. The fluid–rock reactions of greatest significance within fault zones in granitic basement involve the reversible transformations of K-feldspar and/or albite to muscovite. K-feldspar and quartz growth result in fault strengthening, whereas muscovite and chlorite cause fault weakening (Wintsch et al., 1995; Wibberley, 1999). The proportion of these minerals within the host and fault rock will govern the bulk strength of the fault rock (Crawford et al., 2008; Ikari et al., 2011). Muscovite will precipitate in acidic (e.g. low K^+/H^+) fluid conditions, while K-feldspar will form in near neutral conditions (Fig. 10) (Wintsch et al., 1995). The alkali/H^+ ratios can be changed by either deformation, which increases the amount of reactive mineral surfaces, or by the introduction of water, which increases the proportion of H^+ (Wintsch et al., 1995). Depending on the area of new surfaces exposed and the volume of fluid there are three main paths by which the fluid could evolve through time shown in Fig. 10.

1. Deformation associated with a small volume of fluid. The availability of alkalis is greater than H^+, resulting in a rock-dominated system that promotes K-feldspar crystallisation and strengthens the fault.
2. Deformation and a large but finite volume of fluid. An increased volume of fluid produces a fluid-dominated (H^+-rich) system causing muscovite growth. As fluid is used up, the system evolves to be rock-dominated causing K-feldspar formation. Initial fault weakening is followed by strengthening.
3. Permanent supply of fresh fluid. A long-lived fluid-dominated system causes extensive muscovite crystallisation and fault weakening.

9.2. Fault evolution in the Monte Rosa granitic gneiss

The Virgin Fault and Ciao Ciao Fault were both affected by fracturing and cataclasis, but different mineral reactions. K-feldspar, quartz and chlorite are abundant within the Virgin Fault, while muscovite is prevalent in the Ciao Ciao Fault. Microstructural observations show that in both faults, fault core formation occurred by several steps, which had either weakening or strengthening effects. Strengthening of the fault core resulted in discrete fracturing, while weakening processes promoted more pervasive cataclastic flow.

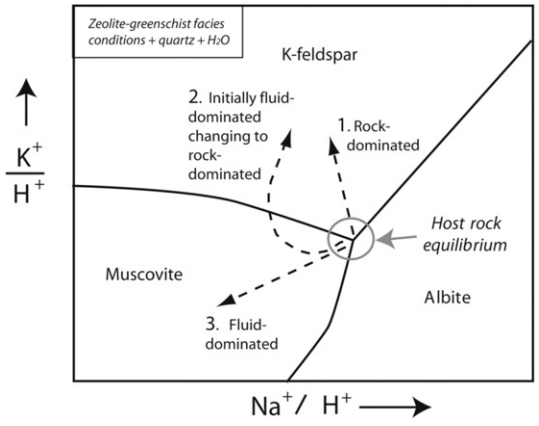

Fig. 10. Schematic fluid activity diagram modified from Wintsch et al. (1995) showing mineral stability of muscovite and feldspar. Paths 1, 2 and 3 represent different fluid–rock ratio conditions. 1) Rock dominated conditions = K-feldspar precipitation. 2) Fluid dominated conditions that evolve to rock dominated conditions = muscovite precipitation followed by K-feldspar precipitation. 3) Fluid dominated conditions = muscovite precipitation.

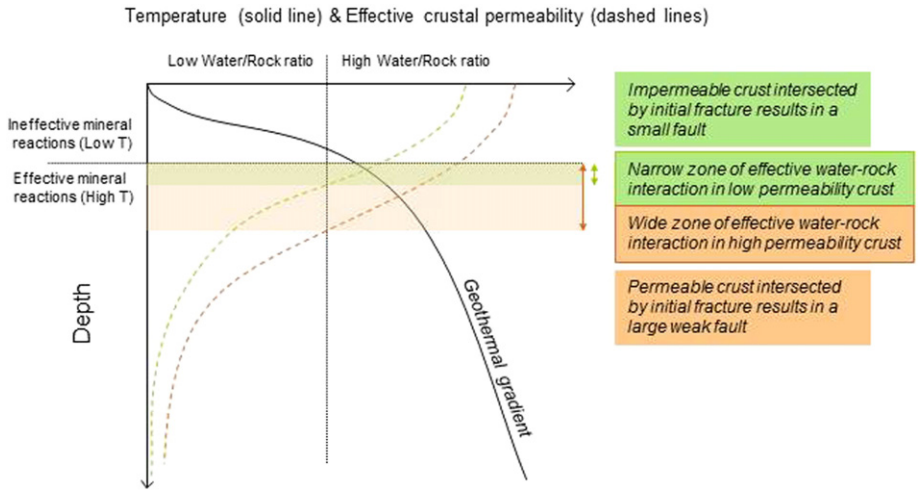

Fig. 11. Schematic representation of geothermal gradient (solid black line) and permeability with depth. Two dashed curves represent either high permeability (orange) or low permeability (green) crust. Green and orange bands represents optimum depth for fault development in low and high permeability crust respectively, requiring a combination of high water:rock ratio (W/R) and elevated temperature. Permeability profiles in the crust from Ingebritsen and Manning (1999).

Mechanical deformation within the Virgin Fault increased permeability and promoted fluid–rock reactions. However due to low permeability and/or a small volume of fluid, the system was rock-dominated and promoted K-feldspar, quartz and chlorite growth (path 1 in Fig. 10). The relative proportion of phyllosilicates to framework silicates was not changed much by these reactions and therefore the strength was not modified greatly. However, reactions did reduce grain size, causing weakening. This ultimately promoted cataclasis, which enabled more fluids to enter and promoted mineral reactions. K-feldspar proportions increased and the cataclasite was cemented causing the rock to acquire strength similar to that of the host rock (Wintsch, 1998), and any further deformation would have occurred through renewed fracturing.

Higher permeability in the Ciao Ciao Fault, perhaps due to a locally initial higher joint density or intersection with a greater range of host lithologies, resulted in the introduction of a larger volume of fluid. This fluid-dominated regime promoted the formation of muscovite (path 3 in Fig. 10), feldspar replacement and quartz dissolution. These changes caused grain size reduction and combined with the generation of muscovite, caused major weakening of the Ciao Ciao Fault. This promoted cataclasis that increased permeability, and the continued fluid-dominated conditions caused further weakening. This persisted until enough muscovite had been generated to enable an interconnected network of phyllosilicates and formation of a well-developed foliation. On short timescales, the foliated cataclasite then acted as a fluid barrier (Jefferies et al., 2006b) which prevented refreshment of the fluids within the foliated zone. The closed system promoted quartz precipitation, which led to increased fluid pressure and fracturing. Thus although the creation of a foliation initially lowered the strength of the fault rock (Wibberley, 1999; Ikari et al., 2011), the foliation subsequently prevented fluid access and strengthened the fault. This difference in mineral reactions created two faults characterised by fundamentally different strengths and deformation histories.

The penetration of meteoric fluids into both faults during exhumation emphasizes the importance of permeable structures extending to depth in the crust. Studies such as that by Edwards and Ratschbacher (2005) and Menzies et al. (2014) show that high volumes of non-locally derived fluids have played a role in fault mechanics at seismogenic depths. It is tempting to suggest that the cyclic opening of veins within the mylonites of the Ciao Ciao Fault may be related to the seismic cycle. However unequivocal evidence of seismic slip remains limited to fault-related pseudotachylites (Niemeijer et al., 2012). Mineral precipitation and associated fault hardening can be a possible precursor to seismic slip and pseudotachylite production (Di Toro and Pennacchioni, 2005). Although rare fine grained structures with geometries similar to pseudotachylites are locally present (Lawther, 2011), they lack many of the key diagnostic features (Price et al., 2012) and are difficult to confidently identify.

10. A conceptual model for fault evolution in granitic basement

- Faults are likely to have initiated on pre-existing joints and so the initial strength is reduced compared to the intact host rock. Those faults that nucleate in regions of high joint intensity or orientation variability, which are consequently forming better linked networks, may develop greater initial permeability. This initial difference may strongly influence their evolution.
- Fracturing and/or cataclasis will decrease the rock strength. In the fracture systems with lower permeability, K-feldspar formation strengthens the rock to a similar value to the host rock (Wintsch, 1998). Many faults may not evolve past this stage.
- Further fracturing increases permeability and fluid/rock ratios and both muscovite and K-feldspar form. An increased proportion of muscovite gradually weakens the fault, however this is countered by K-feldspar precipitation.
- High permeability allows muscovite precipitation to dominate and significant weakening occurs with the development of an interconnected foliation. A step change in fault architecture occurs, typified by a major increase in width and length. A transition into higher fluid/rock ratios may be linked to higher permeability associated with deformation processes alone. Equally the growing fault may intersect more permeable lithologies or levels in the crust where fluids are more readily available. This could occur through fault propagation or due to exhumation during faulting.
- Foliation development may result in quartz precipitation; an associated disruption to the foliation; an increase in fault strength; fracturing and ingress of fresh reactive fluids promoting muscovite growth and further foliation development. The fault will experience cycles of increased and decreased strength.
- With continued growth of larger faults, deformation is localised onto fewer faults causing the deactivation of smaller faults (Martel et al., 1988; Martel, 1990; Walsh et al., 2003). The “death” of smaller faults is therefore likely to be in part controlled by the behaviour of the other faults within the population.

The evolution of fault strength during the lifetime of a fault population will differ for a small, simple fault or a compound fault. The implication of the different evolution of the larger Ciao Ciao fault and smaller Virgin Fault in very similar host rocks is that small faults as currently seen do not represent the initial stages of formation of larger faults. Some small faults will develop into large faults, others are destined to remain small because of their initial characteristics. Our findings at Monte Rosa show that small faults record fundamentally different fluid–rock reactions to large faults. From this we hypothesize that the strength of small and large faults and consequently their structural evolution are also fundamentally different.

Whilst host rock strength and rheology is an important control on the initial development of the fracture systems, we conclude that effective crustal permeability coupled to ambient temperature may be of more importance to the evolution of faults at depth. Effective crustal permeability will be constrained by the most permeable lithology or structure that intersects the fault zone. Hence fractures with high water/rock ratios may evolve into large fault zones, if temperatures are sufficient for repeated phases of muscovite formation. This evolution will depend on the time that faults spend within the reactive and permeable crustal "zone" (Fig. 11). Within rapidly exhuming crustal sections faults will spend less time in the zone of effective water–rock interaction and hence may have less opportunity to develop the weak mineralogy that will characterise the larger fault zones in granitic basement rocks. The weaker and hence larger fault zones will inevitably intersect more permeable horizons and this feedback mechanism should create a size – frequency distribution for fault populations characterised by numerous small low displacement faults and rare large displacement faults.

Acknowledgements

The research was supported by a NERC studentship NE/F007671/1 and a NERC Isotope Geoscience Facility award IP-1156-1109. Isotopic analysis was performed at the Scottish Universities Environmental Research Centre. Peter Chung, John Gilleece, Craig Barrie, Terry Donnelly, Robert and Alison McDonald are thanked for technical assistance. AJB is funded by NERC support of the NERC Isotope Community Support Facility (R8/H10/76) and SUERC. Two anonymous reviewers provided constructive comments.

References

Amato, J.M., Johnson, C.M., Baumgartner, L.P., Beard, B.L., 1999. Rapid exhumation of the Zermatt-Saas ophiolite deduced from high-precision SmNd and RbSr geochronology. Earth Planet. Sci. Lett. 171, 425–438.

Baker, A.J., 1990. Stable isotopic evidence for fluid–rock interactions in the Ivrea Zone, Italy. J. Petrol. 31, 243–260.

Barker, A.J., Bennett, D.G., Boyce, A.J., Fallick, A.E., 2000. Retrogression by deep infiltration of meteoric fluids into thrust zones during late-orogenic rapid unroofing. J. Metamorph. Geol. 18, 307–318.

Bearth, P., 1952. Geologie und Petrographie des Monte Rosa. Beitr. Geol. Karte Schweiz 96 (94 pp.).

Berger, A., Bousquet, R., 2008. Subduction-related metamorphism in the Alps: review of isotopic ages based on petrology and their geodynamic consequences. Geol. Soc. Lond., Spec. Publ. 298, 117–144.

Bird, D.K., Spieler, A.R., 2004. Epidote in geothermal systems. Rev. Mineral. Geochem. 56, 235–300.

Bistacchi, A., Eva, E., Massironi, M., Solarino, S., 2000. Miocene to Present kinematics of the NW-Alps: evidence from remote sensing, structural analysis, seismotectonics and thermochronology. J. Geodyn. 30, 205–228.

Bocquet, J., Delaloye, M., Hunziker, J.C., Krummenacher, D., 1974. K–Ar and Rb–Sr dating of blue amphiboles, micas, and associated minerals from the Western Alps. Contrib. Mineral. Petrol. 47, 7–26.

Bodnar, R.J., 1993. Revised equation and table for determining the freezing point depression of H_2O–NaCl solutions. Geochim. Cosmochim. Acta 57, 683–684.

Bodnar, R., Vityk, M., 1994. Interpretation of microthermometric data for H_2O–NaCl fluid inclusions. In: De Vivo, B., Frezzotti, M.L. (Eds.), Fluid Inclusions in Minerals, Methods and Applications. Virginia Tech, Blacksburg, VA, pp. 117–130.

Boulton, C., Davies, T., McSaveney, M., 2009. The frictional strength of granular fault gouge: application of theory to the mechanics of low-angle normal faults. Geol. Soc. Lond., Spec. Publ. 321, 9–31.

Bowers, T.S., Taylor, H.P., 1985. Integrated chemical and stable isotope model of the origin of midocean ridge hot spring systems. J. Geophys. Res. 90, 12583–12606.

Burgess, R., Kelley, S.P., Parsons, I., Walker, F.D.L., Worden, R.H., 1992. $^{40}Ar/^{39}Ar$ analysis of perthite microtextures and fluid inclusions in alkali feldspars from the Klokken syenite, South Greenland. Earth Planet. Sci. Lett. 109, 147–167.

Caine, J.S., Evans, J.P., Forster, C.B., 1996. Fault zone architecture and permeability structure. Geology 24, 1025–1028.

Cavailhes, T., Soliva, R., Labaume, P., Wibberley, C., Sizun, J.-P., Gout, C., Charpentier, D., Chauvet, A., Scalabrino, B., Buatier, M., 2013. Phyllosilicate formation in faults rocks: Implications for dormant fault-sealing potential and fault strength in the upper crust. Geophys. Res. Lett. 40, 4272–4278.

Chester, F.M., Evans, J.P., Biegel, R.L., 1993. Internal structure and weakening mechanisms of the San Andreas Fault. J. Geophys. Res. 98, 771–786.

Crawford, B.R., Faulkner, D.R., Rutter, E.H., 2008. Strength, porosity, and permeability development during hydrostatic and shear loading of synthetic quartz-clay fault gouge. J. Geophys. Res. 113, B03207.

Criss, R.E., Taylor Jr., H.P., 1986. Meteoric hydrothermal systems. In: Valley, J.W., Taylor Jr., H.P., O'Neil, J.R. (Eds.), Stable Isotopes in High Temperature Geological Processes. Reviews in Mineralogy 16, pp. 373–424.

Criss, R.E., Gregory, R.T., Taylor Jr., H.P., 1987. Kinetic theory of oxygen isotopic exchange between minerals and water. Geochim. Cosmochim. Acta 51, 1099–1108.

Curti, E., 1987. Lead and oxygen isotope evidence for the origin of the Monte Rosa gold lode deposits (Western Alps, Italy); a comparison with Archean lode deposits. Econ. Geol. 82, 2115–2140.

Dal-Piaz, G.V., Hunziker, J.C., Martinotti, G., 1972. La Zona Sesia-Lanzo e l'evoluzione tettonico-metamorfica delle Alpi nordoccidentali interne. Mem. Soc. Geol. Ital. 11, 433–460.

Di Toro, G., Pennacchioni, G., 2005. Fault plane processes and mesoscopic structure of a strong-type seismogenic fault in tonalites (Adamello batholith, Southern Alps). Tectonophysics 402, 55–80.

Donnelly, T., Waldron, S., Tait, A., Dougans, J., Bearhop, S., 2001. Hydrogen isotope analysis of natural abundance and deuterium-enriched waters by reduction over chromium on-line to a dynamic dual inlet isotope-ratio mass spectrometer. Rapid Commun. Mass Spectrom. 15, 1297–1303.

Edwards, M.A., Ratschbacher, L., 2005. Seismic and aseismic weakening effects in transtension: field and microstructural observations on the mechanics and architecture of a large fault zone in southeastern Tibet. In: Bruhn, D., Burlini, L. (Eds.), High Strain Zones in Nature and Experiment. Geological Society of London Special Publication 245, pp. 109–141.

Evans, J.P., Forster, C.B., Goddard, J.V., 1997. Permeability of fault-related rocks, and implications for hydraulic structure of fault zones. J. Struct. Geol. 19, 1393–1404.

Faulkner, D.R., Mitchell, T.M., Rutter, E.H., Cembrano, J., 2008. On the structure and mechanical properties of large strike-slip faults. Geol. Soc. Lond., Spec. Publ. 299, 139–150.

Fitzgerald, J.D., Stünitz, H., 1993. Deformation of granitoids at low metamorphic grade. 1: Reactions and grain size reduction. Tectonophysics 221, 269–297.

Frey, M., Hunziker, J.C., O'Neil, J.R., Schwander, H.W., 1976. Equilibrium–disequilibrium relations in the Monte Rosa Granite, Western Alps: petrological, Rb–Sr and stable isotope data. Contrib. Mineral. Petrol. 55, 147–179.

Giletti, B., 1986. Diffusion effects on oxygen isotope temperatures of slowly cooled igneous and metamorphic rocks. Earth Planet. Sci. Lett. 77, 218–228.

Gleeson, S.A., Roberts, S., Fallick, A.E., Boyce, A.J., 2008. A combined micro Fourier Transform Infrared (FT-IR) and δD isotopic investigation of hydrothermal vein quartz: Implications for the interpretation of fluid inclusion δD values in hydrothermal systems. Geochim. Cosmochim. Acta 72, 4595–4606.

Goddard, J.V., Evans, J.P., 1995. Chemical changes and fluid–rock interaction in faults of crystalline thrust sheets, northwestern Wyoming, U.S.A. J. Struct. Geol. 17, 533–547.

Graham, C.M., Viglino, J.A., Harmon, R.S., 1987. Experimental-study of hydrogen-isotope exchange between aluminous chlorite and water and of hydrogen diffusion in chlorite. Am. Mineral. 72, 566–579.

Hirth, G., Tullis, J., 1992. Dislocation creep regimes in quartz aggregates. J. Struct. Geol. 14, 145–159.

Hirth, G., Tullis, J., 1994. The brittle–ductile transition in experimentally deformed quartz aggregates. J. Geophys. Res. 99, 11731–11747.

Hurford, A.J., Hunziker, J.C., Stockhert, B., 1991. Constraints on the late thermotectonic evolution of the Western Alps—evidence for episodic rapid uplift. Tectonics 10, 758–769.

Ikari, M.J., Niemeijer, A.R., Marone, C., 2011. The role of fault zone fabric and lithification state on frictional strength, constitutive behavior, and deformation microstructure. J. Geophys. Res. 116, B08404.

Ingebritsen, S.E., Manning, C.E., 1999. Geological implications of a permeability–depth curve for the continental crust. Geology 27, 1107–1110.

Janecke, S.U., Evans, J.P., 1988. Feldspar-influenced rock rheologies. Geology 16, 1064–1067.

Janssen, C., Laube, N., Bau, M., Gray, D.R., 1998. Fluid regime in faulting deformation of the Waratah Fault Zone, Australia, as inferred from major and minor element analyses and stable isotopic signatures. Tectonophysics 294, 109–130.

Jefferies, S.P., Holdsworth, R.E., Shimamoto, T., Takagi, H., Lloyd, G.E., Spiers, C.J., 2006a. Origin and mechanical significance of foliated cataclastic rocks in the cores of crustal-scale faults: Examples from the Median Tectonic Line, Japan. J. Geophys. Res. 111, B12303.

Jefferies, S.P., Holdsworth, R.E., Wibberley, C.A.J., Shimamoto, T., Spiers, C.J., Niemeijer, A.R., Lloyd, G.E., 2006b. The nature and importance of phyllonite development in crustal-scale fault cores: an example from the Median Tectonic Line, Japan. J. Struct. Geol. 28, 220–235.

Jenkin, G.R.T., Fallick, A.E., Leake, B.E., 1992. A stable isotope study of retrograde alteration in SW Connemara, Ireland. Contrib. Mineral. Petrol. 110, 269–288.

Kirkpatrick, J.D., Shipton, Z.K., 2009. Geologic evidence for multiple slip weakening mechanisms during seismic slip in crystalline rock. J. Geophys. Res. 114, B12401.

Lattanzi, P., Curti, E., Bastogi, M., 1989. Fluid inclusion studies on the gold deposits of the upper Anzasca Valley, northwestern Alps. Econ. Geol. 84, 1382–1397.

Lawther, S. 2011. The effects of fluid flow through faults in granite gneiss exhumed from seismogenic depths. University of Glasgow, unpublished PhD thesis. 243 pp.
Logan, J.M., Decker, C.L., 1994. Cyclic fluid flow along faults. United States Geological Survey Open File Report, pp. 94–228.
Martel, S.J., 1990. Formation of compound strike-slip fault zones, Mount Abbot quadrangle, California. J. Struct. Geol. 12, 869–882.
Martel, S.J., Pollard, D.D., Segall, P., 1988. Development of simple strike-slip fault zones, Mount Abbot quadrangle, Sierra Nevada, California. Geol. Soc. Am. Bull. 100, 1451–1465.
Matsuhisa, Y., Goldsmith, J.R., Clayton, R.N., 1979. Oxygen isotopic fractionation in the system quartz–albite–anorthite–water. Geochim. Cosmochim. Acta 43, 1131–1140.
Menzies, C.D., Teagle, D.A.H., Craw, D., Cox, S.C., Boyce, A.J., Barrie, C.D., Roberts, S., 2014. Incursion of meteoric waters into the ductile regime in an active orogeny. Earth Planet. Sci. Lett. 399, 1–13.
Mittempergher, S., Pennacchioni, G., Di Toro, G., 2009. The effects of fault orientation and fluid infiltration on fault rock assemblages at seismogenic depths. J. Struct. Geol. 31, 1511–1524.
Niemeijer, A., Di Toro, G., Griffith, W.A., Bistacchi, A., Smith, S.A.F., Nielsen, S., 2012. Inferring earthquake physics and chemistry using an integrated field and laboratory approach. J. Struct. Geol. 39, 2–36.
O'Hara, K.D., 2007. Reaction weakening and emplacement of crystalline thrusts: diffusion control on reaction rates and strain rate. J. Struct. Geol. 29, 1301–1314.
Ohmoto, H., Rye, R.O., 1974. Hydrogen and oxygen isotopic compositions of fluid inclusions in Kuroko deposits, Japan. Econ. Geol. 69, 947–953.
O'Neil, J.R., Taylor Jr., H.P., 1967. The oxygen isotope cation exchange chemistry of feldspars. Am. Mineral. 52, 1414–1437.
Pettke, T., Diamond, L.W., Villa, I.M., 1999. Mesothermal gold veins and metamorphic devolatilization in northwestern Alps: the temporal link. Geology 27, 641–644.
Price, N.A., Johnson, S.E., Gerbi, C.C., West Jr., D.P., 2012. Identifying deformed pseudotachylyte and its influence on the strength and evolution of a crustal shear zone at the base of the seismogenic zone. Tectonophysics 518–521, 63–83.
Sharp, Z.D., 1990. A laser-based microanalytical method for the insitu determination of oxygen isotope ratios of silicates and oxides. Geochim. Cosmochim. Acta 54, 1353–1357.
Sheppard, S.M.F., 1986. Characterization and isotopic variations in natural waters. In: Valley, J.W., Taylor Jr., H.P., O'Neil, J.R. (Eds.), Stable Isotopes in High Temperature Geological Processes. Reviews in Mineralogy 16, pp. 165–184.
Shepherd, T.J., Rankin, A.H., Alderton, D.M.H., 1985. A practical guide to fluid inclusion studies. Blackie & Son Ltd., Glasgow.
Stipp, M., Stünitz, H., Heilbronner, R., Schmid, S.M., 2002. The eastern Tonale fault zone: a "natural laboratory" for crystal plastic deformationof quartz over a temperature range from 250 to 700 °C. J. Struct. Geol. 24, 1861–1884.
Suzuoki, T., Epstein, S., 1976. Hydrogen isotope fractionation between OH-bearing minerals and water. Geochim. Cosmochim. Acta 40, 1229–1240.
Taylor Jr., H.P., 1977. Water/rock interactions and the origin of H_2O in granitic batholiths. J. Geol. Soc. Lond. 133, 509–558.
Tullis, J., Yund, R.A., 1985. Dynamic recrystallization of feldspar—a mechanism for ductile shear zone formation. Geology 13, 238–241.
Vennemann, T.W., O'Neil, J.R., 1996. Hydrogen isotope exchange reactions between hydrous minerals and molecular hydrogen: I. A new approach for the determination of hydrogen isotope fractionation at moderate temperatures. Geochim. Cosmochim. Acta 60, 2437–2451.
Verdel, C., Niemi, N., van der Pluijm, B.A., 2011. Variations in the illite to muscovite transition related to metamorphic conditions and detrital muscovite content: insight from the Paleozoic passive margin of southwestern United States. J. Geol. 119, 419–437.
Walsh, J.J., Childs, C., Imber, J., Manzocchi, T., Watterson, J., Nell, P.A.R., 2003. Strain localisation and population changes during fault system growth within the Inner Moray Firth, Northern North Sea. J. Struct. Geol. 25, 307–315.
Wenner, D.B., Taylor Jr., H.P., 1976. Oxygen and hydrogen isotope studies of a Precambrian granite–rhyolite terrane, St. Francois Mountains, southeastern Missouri. Geol. Soc. Am. Bull. 87, 1587–1598.
Wibberley, C.A.J., 1999. Are feldspar-to-mica reactions necessarily reaction-softening processes in fault zones? J. Struct. Geol. 21, 1219–1227.
Wintsch, R.P., 1975. Feldspathization as a result of deformation. Geol. Soc. Am. Bull. 86, 35–38.
Wintsch, R.P., 1998. Strengthening of fault breccia by K-feldspar cementation. In: Snoke, A.W., Tullis, J., Todd, V.R. (Eds.), Fault Related Rocks: A Petrographic Atlas. Princeton University Press, Princeton, p. 42.
Wintsch, R.P., Christoffersen, R., Kronenberg, A.K., 1995. Fluid–rock reaction weakening of fault zones. J. Geophys. Res. 100, 13021–13032.
Zhang, S., Tullis, T.E., 1998. The effect of fault slip on permeability and permeability anisotropy in quartz gouge. Tectonophysics 295, 41–52.